Revision n. 1 (August 9th 2024)

Manuelarossiite, $CaPbAlF_7$, a new fluoride from the Vesuvius volcano, Italy

FABRIZIO NESTOLA[1*], ANATOLY V. KASATKIN[2], CRISTIAN BIAGIONI[3], VLADISLAV V. GURZHIY[4], RADEK ŠKODA[5], LISA SANTELLO[1] and ATALI A. AGAKHANOV[2]

[1]*Dipartimento di Geoscienze, Università di Padova, Via Gradenigo 6, I-35131, Padova, Italy*
[2]*Fersman Mineralogical Museum of the Russian Academy of Sciences, Leninsky Prospekt 18-2, 119071 Moscow, Russia*
[3]*Dipartimento di Scienze della Terra, Università di Pisa, Via Santa Maria, 53, I-56126 Pisa, Italy*
[4]*Department of Crystallography, Institute of Earth Sciences, St. Petersburg State University, University Emb. 7/9, 199034 Saint-Petersburg, Russia*
[5]*Department of Geological Sciences, Faculty of Science, Masaryk University, Kotlářská 2, 611 37, Brno, Czech Republic*

**e-mail address*: fabrizio.nestola@unipd.it

This is a 'preproof' accepted article for Mineralogical Magazine. This version may be subject to change during the production process.
DOI: 10.1180/mgm.2024.59

ABSTRACT

Manuelarossiite, ideally $CaPbAlF_7$, is a new fluoride mineral found in a specimen from a fumarole formed subsequent to the 1944 eruption of the Vesuvius volcano, Naples Province, Campania, Italy. It occurs as very rare tabular crystals, up to 0.06 × 0.04 × 0.015 mm, in the vugs of volcanic scoria, associated to cerussite. In the same scoria where manuelarossiite was found, anglesite, artroeite, atacamite, calcioaravaipaite, cerussite, challacolloite, cotunnite, hephaistosite, matlockite, napoliite and susannite were identified. Manuelarossiite is colorless with white streak and adamantine lustre. It is brittle and has a laminated fracture. Cleavage is perfect on {001}. D_{calc} = 5.095 g cm^{-3}. The calculated mean refractive index is 1.625. Chemical composition (wt.%, electron microprobe, H_2O calculated by stoichiometry) is: CaO 13.98, PbO 55.46, Al_2O_3 12.59, F 29.45, H_2O 1.68, –O=F –12.40, total 100.76. The empirical formula calculated on the basis of 7 anions is $Ca_{1.00}Pb_{1.00}Al_{1.00}[F_{6.25}(OH)_{0.75}]_{\Sigma 7.00}$. Raman spectroscopy confirms the limited presence of OH^- groups in the mineral. Manuelarossiite is monoclinic, space group *C*2/*m*, with *a* = 7.6754(3), *b* = 7.4443(4), *c* = 9.2870(5) Å, β = 93.928(5)°, *V* = 529.39(5) Å^3 and *Z* = 4. The strongest lines of the powder X-ray diffraction pattern [*d*, Å (*I*, %) (*hkl*)] are: 9.257 (57) (001); 4.537 (72) (111); 3.725 (98) (020); 3.630 (57) (20-1); 3.588 (65) (11–2); 3.460 (100) (021); 3.422 (63) (112); 2.673 (65) (220). The crystal structure was refined to R_1 = 0.056 for 849 reflections with $F > 4\sigma(F)$. It is characterized by {001} layers formed by CaF_8 polyhedra decorated on both sides by AlF_6 octahedra, in turn connected to the {001} layer through edge-sharing. Successive {001} layers are bonded through Pb atoms. The new mineral honors Dr. Manuela Rossi (b. 1977) from the University of Naples for her contribution to the study of the Vesuvius volcano and its minerals.

Keywords: manuelarossiite; fluoride; Raman spectroscopy; crystal structure; 1944 eruption; Vesuvius volcano; Italy.

https://doi.org/10.1180/mgm.2024.59 Published online by Cambridge University Press

Introduction

The Vesuvius volcano in Italy is one of the most scientifically studied volcanoes in the world. Despite the fact that there are no new eruptions since 1944, its list of minerals continues to be regularly updated, both with mineral species new to the locality and those completely new to science in general (Campostrini and Gramaccioli, 2005; Campostrini *et al.*, 2005; Russo and Campostrini, 2011; Campostrini *et al.*, 2019; Demartin *et al.*, 2014; Russo *et al.*, 2014). This happens primarily as a result of the re-examination of old samples by modern analytical techniques. The most recent example is the discovery and characterization of the new mineral napoliite, Pb_2OFCl, in a sample collected more than a decade ago from one of the fumaroles of the 1944 eruption. Two other minerals, hephaistosite and susannite, were found in the same association for the first time at Vesuvius (Kasatkin *et al.*, 2023).

Manuelarossiite, described in this article, represents the 68th mineral species for which the Somma-Vesuvius volcanic complex is the type locality. The new mineral honors Dr. Manuela Rossi (born 28.11.1977), a researcher at the Dipartimento di Scienze della Terra, dell'Ambiente e delle Risorse, Università degli Studi di Napoli Federico II (Naples, Italy), for her contribution to the study of the minerals from the Vesuvius volcano (see, e.g., Rossi, 2010; Rossi *et al.*, 2011, 2014, 2016; Malcherek *et al.*, 2014). She also collected and provided to the authors the sample where the new mineral was found. The mineral, its name and symbol (Mnrs) have been approved by the Commission on New Minerals, Nomenclature and Classification of the International Mineralogical Association (IMA No. 2022-097). The holotype specimen is deposited in the collections of the Fersman Mineralogical Museum of the Russian Academy of Sciences, Moscow, Russia with the registration number 5920/1.

In this paper the description of this new mineral species is reported.

Occurrence and physical properties

A complete description of the environment where manuelarossiite was discovered is extensively provided in the type description of napoliite, a new species found in the same scoria as manuelarossiite by Kasatkin *et al.* (2023). In 2020, our research team started the investigation of a sample of lava scoria collected by Dr. Manuela Rossi in the early 2010s from a large fragment located at the eastern rim of the "Gran Cono" crater. This research project not only resulted in the discovery of both napoliite and manuelarossiite, but the occurrence of further new minerals within the same sample cannot be excluded.

Manuelarossiite overgrows volcanic scoria and is intimately associated with cerussite. In the same scoria where manuelarossiite was found, anglesite, artroeite, atacamite, calcioaravaipaite, cerussite, challacolloite, cotunnite, hephaistosite, matlockite, napoliite and susannite were identified.

Manuelarossiite occurs as very rare tabular crystals, up to 0.06 × 0.04 × 0.015 mm (but usually much smaller), in the vugs of volcanic scoria. Crystals are individual or grouped in clusters (Fig. 1a, b). Manuelarossiite crystals are flattened on {001}; other forms are {100}, {101}, {110}, {111}, {0–10}, {0–11}, {1–10}, {1–11} and {–1–11} (Fig. 2). Twinning along {001} is observed. The new mineral is colorless and transparent with white streak and adamantine lustre. It is brittle and has a laminated fracture. No fluorescence is observed under long- or short-wave ultraviolet light. The hardness could not be measured because of the tiny

https://doi.org/10.1180/mgm.2024.59 Published online by Cambridge University Press

crystal size but is estimated at 2 – 3 on the Mohs' scale by analogy with other lead aluminofluorides (e.g., aravaipaite, artroeite, calcioaravaipaite). Cleavage is perfect on {001}. The density calculated using the empirical formula and unit-cell volume obtained from single-crystal X-ray diffraction data is 5.095 g cm^{-3}. The optical properties of manuelarossiite cannot be measured due to the extremely small size and thinness of its crystals. A mean index of refraction calculated on the basis of Gladstone-Dale equation is 1.625.

Chemical and spectroscopic data

Quantitative chemical analyses were carried out using a Cameca SX 100 electron microprobe (WDS mode, 15 kV, 4 nA, 2 μm beam diameter) at the Department of Geological Sciences, Faculty of Science, Masaryk University, Brno, Czech Republic. Results (average of 5 spot analyses) are given in Table 1. Determination of the F content was done using PC1 monochromator ($2d$ = 60 Å) and a special care (peak maxima position, background selection) was taken prior the analysis. Both the crystal structure data and Raman spectroscopy (see below) confirm the presence of small amount of $(OH)^-$ groups in the mineral and the absence of H_2O, borate and carbonate groups. The contents of other elements with atomic numbers higher than that of C are below detection limits. X-phi matrix correction (Merlet 1994) was applied to the data. The empirical formula (calculated on the basis of 7 anions) is: $Ca_{1.00}Pb_{1.00}Al_{1.00}[F_{6.25}(OH)_{0.75}]_{\Sigma 7.00}$. The ideal formula is $CaPbAlF_7$, which requires CaO 13.77, PbO 54.80, Al_2O_3 12.52, F 32.66, –O=F –13.75, total 100.00 wt.%

The Raman spectrum of manuelarossiite (Fig. 3) was collected in the range 100 – 4000 cm^{-1} using a WITec alpha300 R Raman Imaging Microscope equipped with a green laser (532 nm, grating 300 gr/mm) and a 50× LWD (long working distance) objective at the Department of Geosciences of the University of Padova, Italy. The data were collected using a laser power of 6 mW for 30 seconds of integration time and 4 accumulations.

The Raman spectrum of manuelarossiite shows the most intense band at 560 cm^{-1} accompanied by an intense shoulder at 540 cm^{-1}, whereas lower intensity bands (at least 10) are located in the region between about 120 and 425 cm^{-1}. A significant band is also located at 650 cm^{-1}. In the O–H stretching region (see inset in Fig. 3), one single band at 3604 cm^{-1} is present with an intensity about eight times lower than that of the most intense band at 560 cm^{-1}. No bands are observed in the range 700 – 3500 cm^{-1}.

The Raman spectrum of manuelarossiite can be directly compared with the spectrum published for calcioaravaipaite $PbCa_2AlF_9$ (Kampf *et al.*, 2011). For manuelarossiite, the same band assignments done for calcioaravaipaite can be adopted, with the Raman bands between 100 and 200 cm^{-1} that could be assigned to complex vibration modes of Ca–O and Pb–O, those between 200 and 400 cm^{-1} assigned to the F–Al–F bending vibrations, and with the main two bands at 560 and 540 cm^{-1} likely related to the stretching vibrations of the AlF_6 octahedra. The band at 650 cm^{-1} could be assigned to the (Ca,Pb)–OH stretching vibrations. The low intensity of the 3604 cm^{-1} band is consistent with a limited presence of $(OH)^-$ anion. The O–H stretching position in manuelarossiite is consistent with the position at 3582 cm^{-1} for calcioaravaipaite (Kampf *et al.*, 2011).

X-ray crystallography

https://doi.org/10.1180/mgm.2024.59 Published online by Cambridge University Press

Powder X-ray diffraction (XRD) data were collected with a Rigaku R-AXIS Rapid II single-crystal diffractometer equipped with a cylindrical image plate detector using the Debye-Scherrer geometry (d = 127.4 mm), Co$K\alpha$ radiation (rotating anode with VariMAX microfocus optics), 40 kV and 15 mA. The angular resolution of the detector is 0.045° 2θ (pixel size 0.1 mm). The data were integrated using the software package *Osc2Tab* (Britvin *et al.*, 2017). The powder XRD data of manuelarossiite are given in Table 2 in comparison to that calculated from single-crystal XRD data using the *Vesta* program (Momma and Izumi, 2011). Unit-cell parameters from the powder data were calculated from the observed d spacing data using *UnitCell* software (Holland and Redfern, 1997) and are as follows: a = 7.682(2), b = 7.454(2), c = 9.284(2) Å, β = 93.93(3)°, V = 530.4(2) Å^3 and Z = 4.

To obtain single-crystal XRD data, a small tabular crystal of manuelarossiite was mounted on a thin glass fiber and examined using a Supernova Rigaku-Oxford Diffraction single-crystal diffractometer (Mo$K\alpha$ radiation, 50 kV and 0.12 mA working conditions) equipped with a Pilatus 200 K Dectris detector. The detector-to-crystal distance was 69 mm. Data were collected by 1707 frames over 30 runs, in 1° slices, with an exposure time of 45 s per frame and a total time of about 20 hours. The data were corrected for Lorentz and polarization factors and absorption using the software package Crysalis Pro (version 41.64.113a). The refined unit-cell parameters of manuelarossiite are the following: a = 7.6754(3), b = 7.4443(4), c = 9.2870(5) Å, β = 93.928(5)°, V = 529.39(5) Å^3.

The crystal structure of manuelarossiite was solved through direct methods using *Shelxs*-97 (Sheldrick, 2015) and refined through *Shelxl*-2018 (Sheldrick, 2015). After having located the heavier atoms, the positions of the remaining atoms were identified through successive difference-Fourier maps. Three cation and five anion positions were found. Neutral scattering curves, taken from the *International Tables for Crystallography* (Wilson, 1992), were used. Twinning on {001} was modelled, giving a ratio between the two individuals of 0.044(2). During the final stages of the refinement, the Pb site was found to be split into two sub-positions, Pb(1a) and Pb(1b). Moreover, relatively high residuals in the difference-Fourier maps (up to ca. 7.5 e/Å^3) were observed. These structural features can be due to some difficulties in the appropriate modelling of the absorption using the multi-scan technique or to the possible order-disorder (OD) nature of manuelarossiite, in accord with the OD nature of the related mineral calcioaravaipaite (Kampf *et al.*, 2003). However, notwithstanding this shortcoming, the crystal-chemical features are sound (see below) and the anisotropic structural model of manuelarossiite converged to R_1 = 0.0561 for 849 reflections with $F_o > 4\sigma(F_o)$ and 58 refined parameters. Details of data collection and refinement are given in Table 3. Fractional atomic coordinates and equivalent isotropic displacement parameters are reported in Table 4, whereas Table 5 reports selected bond distances. Table 6 shows bond-valence sums calculated according to the bond-parameters of Brese and O'Keeffe (1991).

Crystal structure description

The crystal structure of manuelarossiite (Figs. 4a and 4b) is characterized by {001} layers formed by CaF_8 polyhedra decorated on both sides by AlF_6 octahedra, connected to the {001} layer through edge-sharing. Average <Ca–F> distance is 2.360 Å, to be compared with the values observed at the two independent Ca sites in calcioaravaipaite, i.e., 2.360 and 2.361 Å, respectively (Kampf *et al.*, 2011). Bond-valence sum at the Ca site is 1.98 valence units (v.u.).

https://doi.org/10.1180/mgm.2024.59 Published online by Cambridge University Press

The Al-centered octahedron has average <Al–F> distance of 1.807 Å, in agreement with the values observed by Kampf *et al.* (2011) in aravaipaite and calcioaravaipaite, i.e., 1.806 and 1.808 Å, respectively. Bond-valence sums at the Al site of manuelarossiite is 2.97 v.u.

Successive {001} layers are bonded through Pb atoms. Lead atoms are mainly hosted at the Pb(1a) [site occupancy factor = 0.963(3)], whereas only minor Pb occurs at the Pb(1b) position [site occupancy factor = 0.037(3)]. Lead atoms at Pb(1a) have an asymmetric bonding environment, with five bond distances shorter than 2.70 Å and seven longer ones, ranging between 2.96 and 3.33 Å. This asymmetry is probably related to the stereoactive nature of the $6s^2$ lone-electron-pair of Pb^{2+}. The average <Pb–F> of the five shortest distances is 2.504 Å, to be compared to 2.511 Å given by Kampf *et al.* (2011) for calcioaravaipaite. The bond-valence sum at Pb(1a), assuming its full-occupancy, is 1.86 v.u. Whereas Pb(1a) has a twelve-fold coordination, Pb(1b) has an eleven-fold coordination, as the PbF_{11} polyhedra reported by Kampf *et al.* (2001) in aravaipaite; also in this case, the coordination environment is asymmetric, with three distances shorter than 2.70 Å. Assuming its full-occupancy by Pb, the bond-valence sum at Pb(1b) is 2.18 v.u.

Five independent F sites occur in manuelarossiite. According to electron microprobe data, 0.75 (OH) groups per formula unit occur. The location of H atom was not possible and only some hypotheses about the actual position of (OH) groups can be put forward. All F sites show bond-valence sums ranging between 0.87 and 1.10 v.u. Three of them, i.e., F(3), F(4), and F(5) have a distorted tetrahedral coordination and the occurrence of an H atom seems unlikely; F(1) and F(2) show a triangular coordination. This situation is similar to what found by Kampf *et al.* (2003) in calcioaravaipaite, where no conclusive evidence for assigning O to any F site was found. Taking into account the results of crystal structure refinement, coupled with electron microprobe data, the crystal chemical formula of manuelarossiite is proposed as $CaPbAl(F,OH)_7$ ($Z = 4$).

Relations with other Pb-Al fluorides

Lead-Al fluoride are currently represented by very few phases, i.e., aravaipaite, $Pb_3AlF_9 \cdot H_2O$ (Kampf *et al.*, 1989; Kampf, 2001; Kampf *et al.*, 2011), artroeite, $PbAlF_3(OH)_2$ (Kampf and Foord, 1995), and calcioaravaipaite, Ca_2PbAlF_9 (Kampf and Foord, 1996; Kampf *et al.*, 2011). Manuelarossiite is the fourth mineral showing Pb, Al, and F as essential chemical constituents (Table 7).

Aravaipaite, artroeite and calcioaravaipaite were first identified on specimens from the Grand Reef mine, Aravaipa Mining District, Graham County, Arizona, U.S.A., at the end of the 1980s and in the mid-1990s, respectively (Kampf *et al.*, 1989; Kampf and Foord, 1995, 1996). Calcioaravaipaite was named for its apparent relations with aravaipaite. Actually, these two species show some differences, discussed by Kampf *et al.* (2011). Moreover, both of them display an OD nature (Kampf *et al.*, 2003; Kampf *et al.*, 2011). After the first American findings, these two species have been reported from the fumaroles of Vesuvius, along with artroeite (Campostrini and Gramaccioli, 2005; Russo and Campostrini, 2022).

Manuelarossiite has structural relations with calcioaravaipaite (Fig. 5). These species belong to a homologous series of layered (Ca/Pb)-Al compounds with structural formula $M^{2+}{}_N PbAlF_{5+2N}$, where M^{2+} = Ca. Manuelarossiite is the $N = 1$ homologue, whereas calcioaravaipaite is the $N = 2$ homologues. Artroeite is chemically identical with the $N = 0$

https://doi.org/10.1180/mgm.2024.59 Published online by Cambridge University Press

homologue of this series, with some (OH) replacing F; however, it shows a different crystal structure, with dimers formed by edge-sharing Al-centered octahedra (Kampf and Foord, 1995).

Geological environment of formation

In the studied sample, manuelarossiite along with artroeite, atacamite, calcioaravaipaite and susannite are the latest minerals occurring in the vugs of volcanic scoria altered by fumarolic gas. All of them contain $(OH)^-$ groups either as a species-defining component (artroeite, atacamite, susannite) or a small admixture partly substituting F (manuelarossiite, calcioaravaipaite). We infer therefore that manuelarossiite was probably formed not as a result of direct crystallization from gaseous phases but as a product of the interactions between earlier-formed high-temperature sublimate Pb-bearing minerals (anglesite, cerussite, cotunnite, matlockite, napoliite), HF-containing fumarolic gas and atmospheric water vapor at relatively low temperatures, presumably not higher than 150° C. Similar trends were previously noted in the literature for OH-bearing minerals found in the active fumaroles of the Tolbachik volcano at Kamchatka Peninsula in Russia (see, e.g., Pekov *et al.*, 2021).

Conclusion

Manuelarossiite is a new addition to the long list of mineral species discovered in fumaroles of active volcanoes, one of the most important kinds of occurrence of new minerals according to Pekov and Pushcharovsky (2023). This mineral is also an interesting improvement of our knowledge about the mineral systematics and crystal-chemistry of Pb-Al fluorides, showing the possible existence of an homologous series involving some of these compounds.

Acknowledgements

M. Rossi is acknowledged for providing us with the studied specimen.

https://doi.org/10.1180/mgm.2024.59 Published online by Cambridge University Press

References

Brese N.E. and O'Keeffe M. (1991) Bond-valence parameters for solids. *Acta Crystallographica*, **B47**, 192–197.

Britvin S.N., Dolivo-Dobrovolsky D.V., and Krzhizhanovskaya M.G. (2017) Software for processing the X-ray powder diffraction data obtained from the curved image plate detector of Rigaku RAXIS Rapid II diffractometer. *Zapiski Rossiiskogo Mineralogicheskogo Obshchestva*, **146**, 104–107 (in Russian).

Campostrini I. and Gramaccioli C. (2005) Artroeite del Monte Somma-Vesuvio: secondo ritrovamento mondiale. *Rivista Mineralogica Italiana*, **29**, 50–52.

Campostrini I., Demartin F., and Russo M. (2019) Sbacchiite, Ca_2AlF_7, a new fumarolic mineral from the Vesuvius volcano, Napoli, Italy. *European Journal of Mineralogy*, **31**, 153–158.

Demartin F., Campostrini I., Castellano C., and Russo M. (2014) Parascandolaite, $KMgF_3$, a new perovskite-type fluoride from Vesuvius. *Physics and Chemistry of Minerals*, **41**, 403–407.

Holland T.J.B. and Redfern S.A.T. (1997) Unit cell refinement from powder diffraction data: the use of regression diagnostics. *Mineralogical Magazine*, **61**, 65–77.

Kampf A.R., Dunn P.J., and Foord E.E. (1989) Grandreefite, pseudograndreefite, laurelite, and aravaipaite: four new minerals from the Grand Reef mine, Graham County, Arizona. *American Mineralogist*, **74**, 927–933.

Kampf A.R. and Foord E.E. (1995) Artroeite, $PbAlF_3(OH)_2$, a new mineral from the Grand Reef mine, Graham County, Arizona: Description and crystal structure. American Mineralogist, **80**, 179–183.

Kampf A.R. and Foord E.E. (1996) Calcioaravaipaite, a new mineral, and associated lead fluoride minerals from the Grand Reef mine, Graham County, Arizona. *Mineralogical Record*, **27**, 293–300.

Kampf A.R. (2001) The crystal structure of aravaipaite. *American Mineralogist*, **86**, 927–931.

Kampf A.R., Merlino S., and Pasero M. (2003) Order-disorder approach to calcioaravaipaite, $[PbCa_2Al(F,OH)_9]$: The crystal structure of the triclinic MDO polytype. *American Mineralogist*, **88**, 430–435.

Kampf A.R., Yang H., Downs R.T., and Pinch W.H. (2011) The crystal structures and Raman spectra of aravaipaite and calcioaravaipaite. *American Mineralogist*, **96**, 402–407.

Kasatkin A.V., Siidra O.I., Nestola F., Pekov I.V., Agakhanov A.A., Koshlyakova N.N., Chukanov N.V., Nazarchuk E.V., Molinari S., and Rossi M. (2023) Napoliite, Pb_2OFCl, a new mineral from Vesuvius volcano, and its relationship with dimorphous rumseyite. *Mineralogical Magazine*, **87**, 711–718.

Malcherek T., Bindi L., Dini M., Ghiara M.R., Molina Donoso A., Nestola F., Rossi M., and Schluter J. (2014) Tondiite, $Cu_3Mg(OH)_6Cl_2$, the Mg-analog of herbertsmithite. *Mineralogical Magazine*, **78**, 583–590.

Merlet C. (1994). An accurate computer correction program for quantitative electron probe microanalysis. *Microchimica acta*, **114**, 363–376.

Momma K. and Izumi F. (2011) VESTA 3 for three-dimensional visualization of crystal, volumetric and morphology data. *Journal of Applied Crystallography*, **44**, 1272-1276.

Pekov I.V. and Pushcharovsky D.Y. (2023) The discovery of new minerals in modern mineralogy: experience, implications and perspectives. In: Bindi, L.; Cruciani, G. (eds)

Celebrating the International Year of Mineralogy. Springer Mineralogy. Springer, Cham, 69–99.

Pekov I.V., Zubkova N.V., Zolotarev A.A., Yapaskurt V.O., Krivovichev S.V., Belakovskiy D.I., Lykova I., Vigasina M.F., Kasatkin A.V., Sidorov E.G. and Pushcharovsky D.Yu. (2021) Dioskouriite, $CaCu_4Cl_6(OH)_4 \cdot 4H_2O$: A New Mineral Description, Crystal Chemistry and Polytypism. *Minerals*, **11**, 90.

Rossi M. (2010) The fluorapatites in volcanic products of Somma-Vesuvius volcanic complex: crystallographic parameters, crystal-chemistry and minerogenetic implications. *Plinius*, **36**, 212–221.

Rossi M., Ghiara M.R., Chita G. and Capitelli F. (2011) Crystal-chemical and structural characterization of fluorapatites in ejecta from Somma-Vesuvius volcanic complex. *American Mineralogist*, **96**, 1828–1837.

Rossi M., Nestola F., Zorzi F., Lanza A., Peruzzo L., Guastoni A. and Kasatkin A. (2014) Ghiaraite: A new mineral from Vesuvius volcano, Naples (Italy). *American Mineralogist*, **99**, 519–524.

Rossi M., Nestola F., Ghiara M.R. and Capitelli F. (2016) Fibrous minerals from Somma-Vesuvio volcanic complex. *Mineralogy and Petrology*, **110**, 471–489.

Russo M. and Campostrini I. (2011) Ammineite, matlockite and post 1944 eruption fumarolic minerals at Vesuvius. *Plinius*, **37**, 312.

Russo M. and Campostrini I. (2022) Elenco delle specie minerali del "Somma-Vesuvio". Miscellanea INGV, 65, 1–33.

Russo M., Campostrini I. and Demartin F. (2014) Fumarolic minerals after the 1944 Vesuvius eruption. In: Cesare B., Erba E., Carmina B., Fascio L., Petti F.M. and Zuccari A., eds., The Future of the Italian Geosciences – The Italian Geosciences of the Future. 87° Congresso della Società Geologica Italiana e 90° Congresso della Società Italiana di Mineralogia e Petrologia, Milan, Italy, September 10–12, 2014. Abstract Book. Rendiconti Online della Società Geologica Italiana, 31, Supplemento n.1.

Sheldrick G.M. (2015) Crystal structure refinement with SHELXL. *Acta Crystallographica*, **C71**, 3–8.

Wilson A.J.C. (editor) (1992) International Tables for Crystallography Volume C: Mathematical, Physical and Chemical Tables. Kluwer Academic Publishers, Dordrecht, The Netherlands.

https://doi.org/10.1180/mgm.2024.59 Published online by Cambridge University Press

Table captions

Table 1. Chemical composition of manuelarossiite.

Table 2. Powder X-ray diffraction data (*d* in Å) of manuelarossiite compared to the calculated pattern from single-crystal data.

Table 3. Summary of crystal data and parameters describing data collection and refinement for manuelarossiite.

Table 4. Sites, Wyckoff positions, site occupancy factors (s.o.f.), fractional atomic coordinates and equivalent isotropic displacement parameters ($Å^2$) for manuelarossiite.

Table 5. Selected bond distances (Å) for manuelarossiite.

Table 6. Weighted bond-valence sums (in valence unit) for manuelarossiite.

Table 7. Comparison between currently known Pb-Al fluorides.

Figure captions

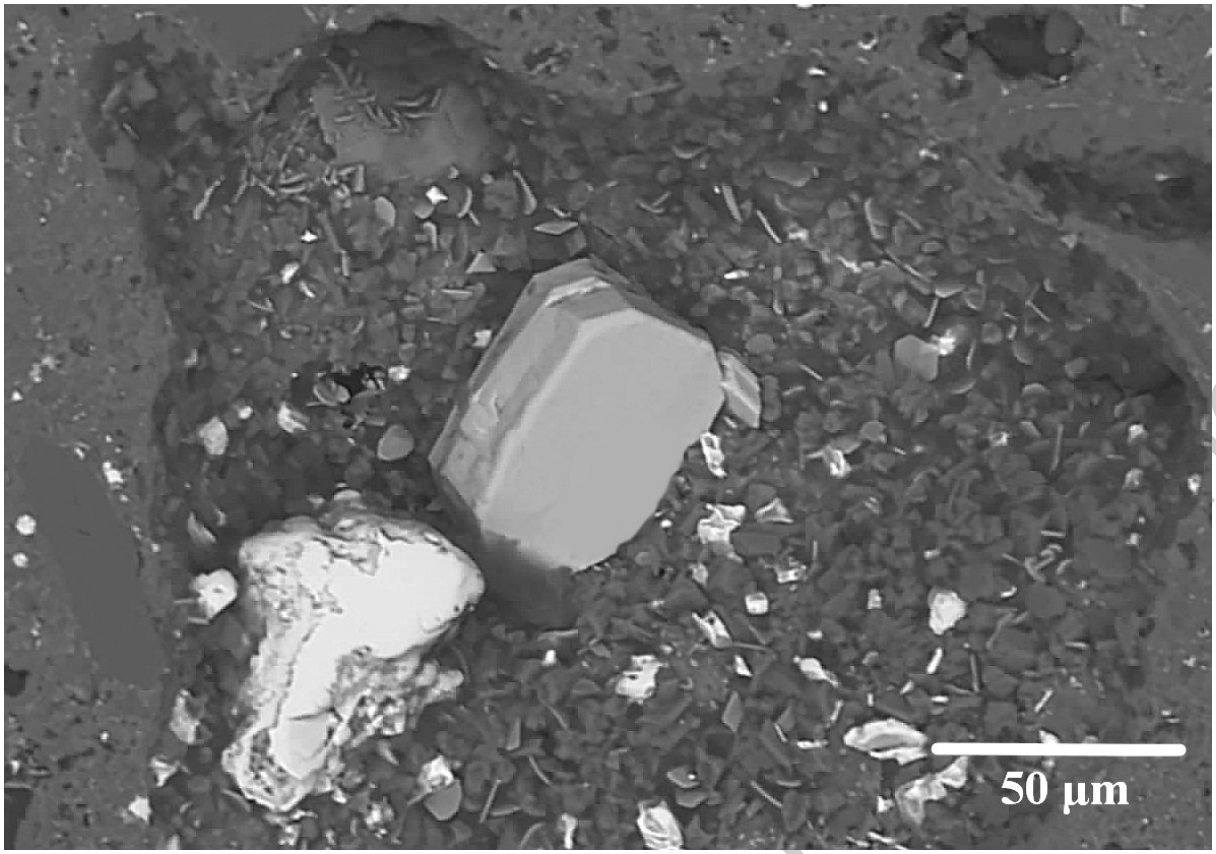

https://doi.org/10.1180/mgm.2024.59 Published online by Cambridge University Press

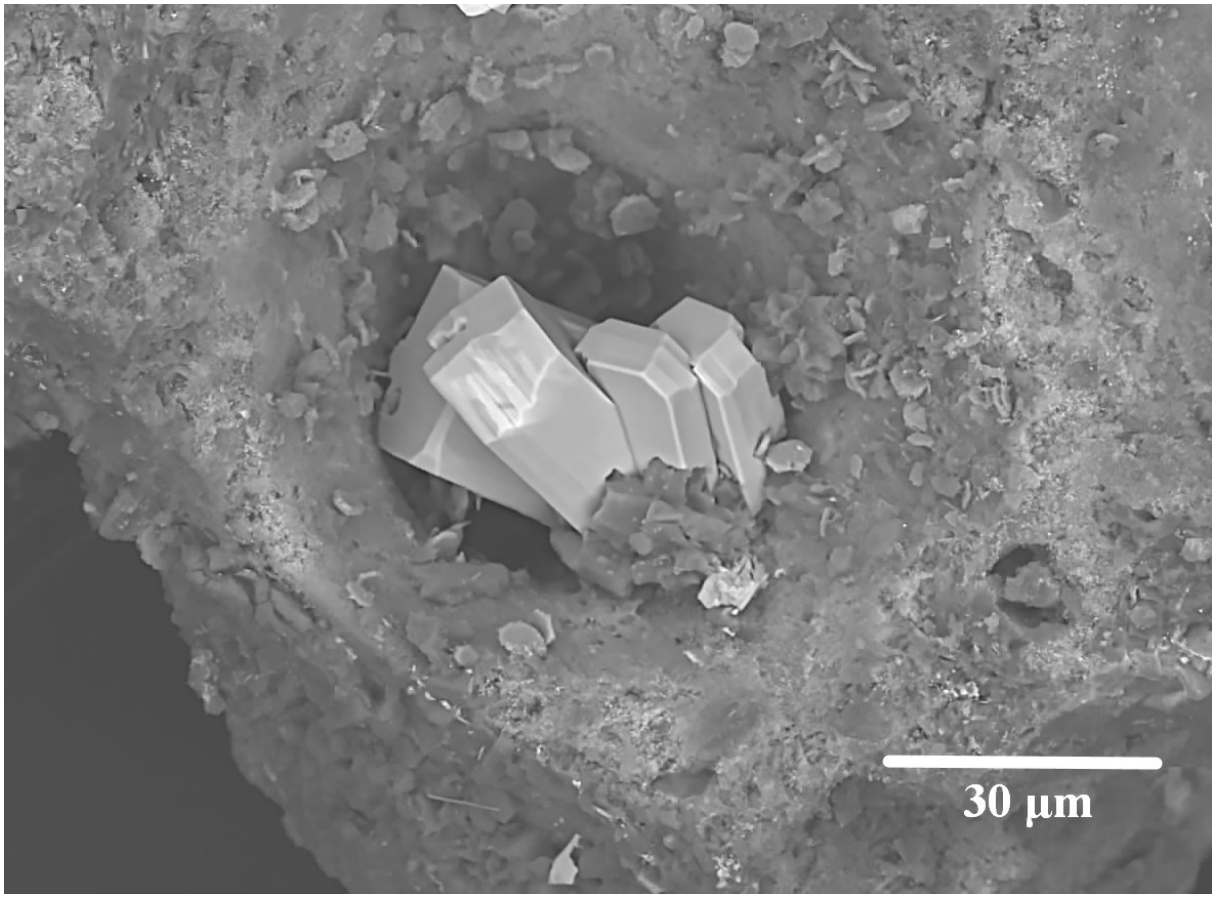

Figure 1. (a) Manuelarossiite tabular crystal (grey in the center) associated to cerussite (white) in a vug of the volcanic scoria; (b) group of manuelarossiite crystals in a vug of the volcanic scoria. SEM (BSE) images.

https://doi.org/10.1180/mgm.2024.59 Published online by Cambridge University Press

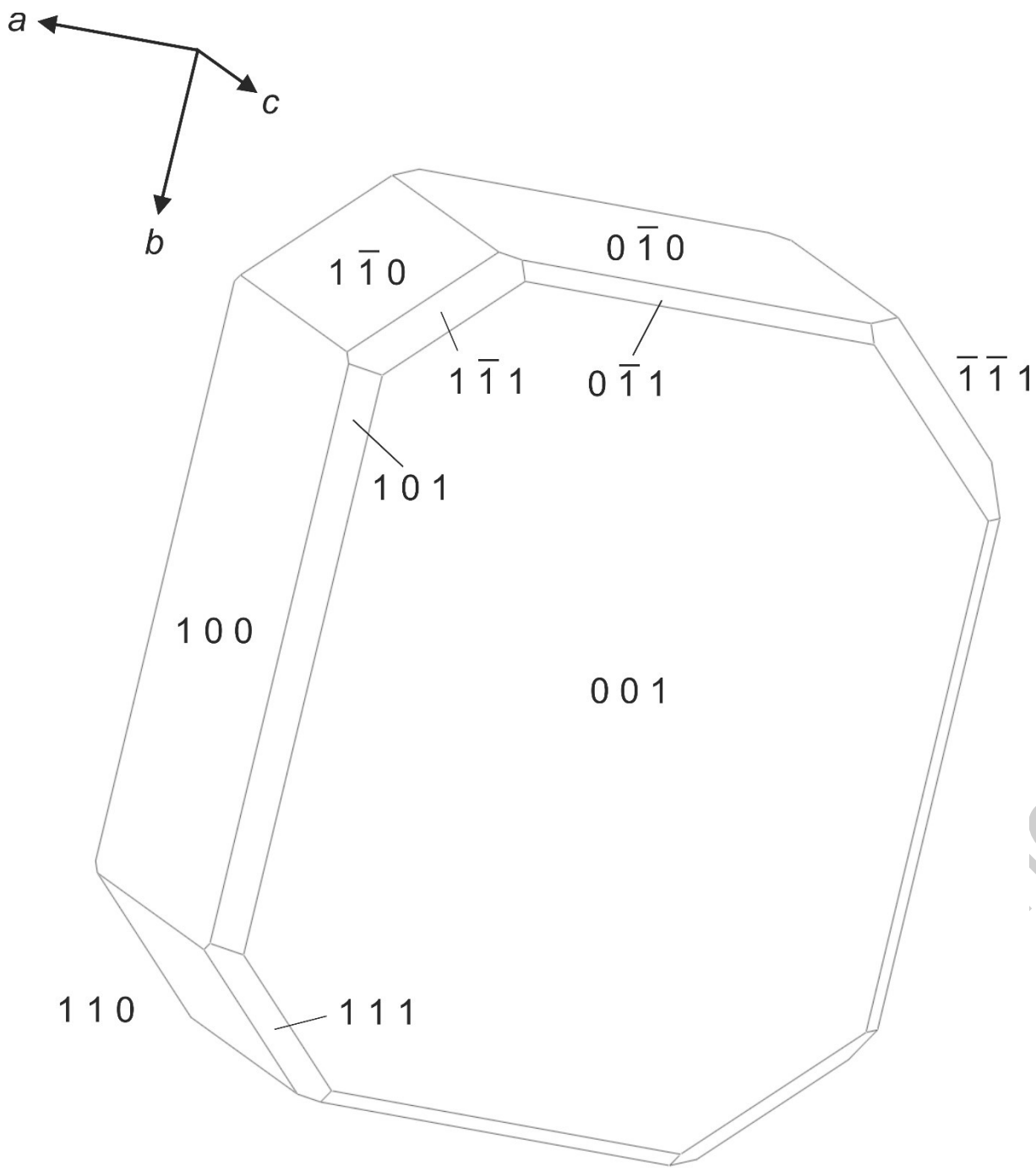

Figure 2. Crystal drawing of manuelarossiite.

https://doi.org/10.1180/mgm.2024.59 Published online by Cambridge University Press

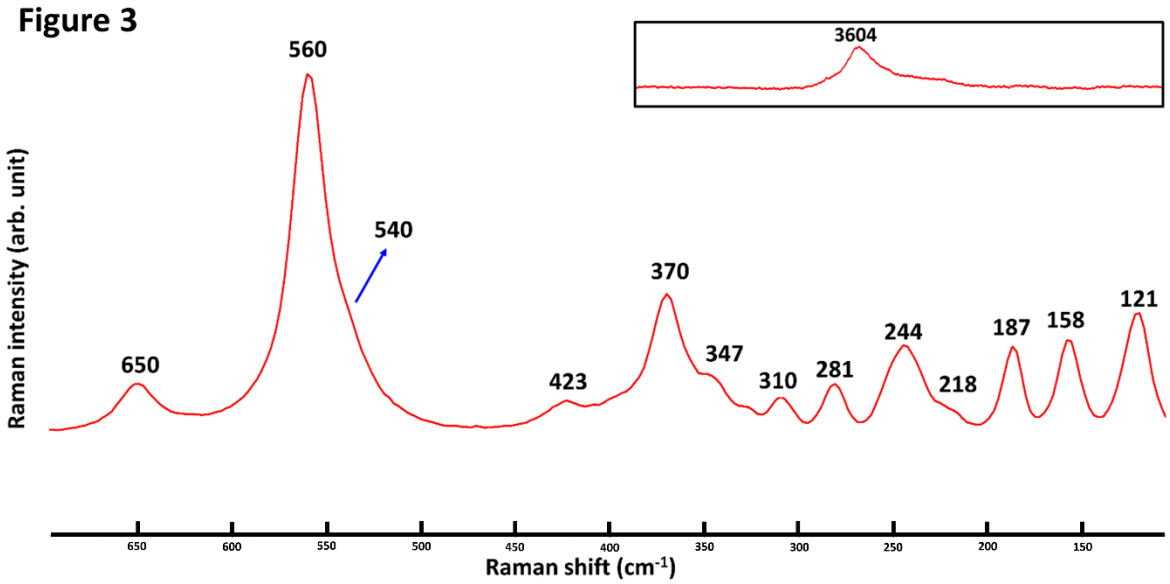

Figure 3. Raman spectrum of manuelarossiite.

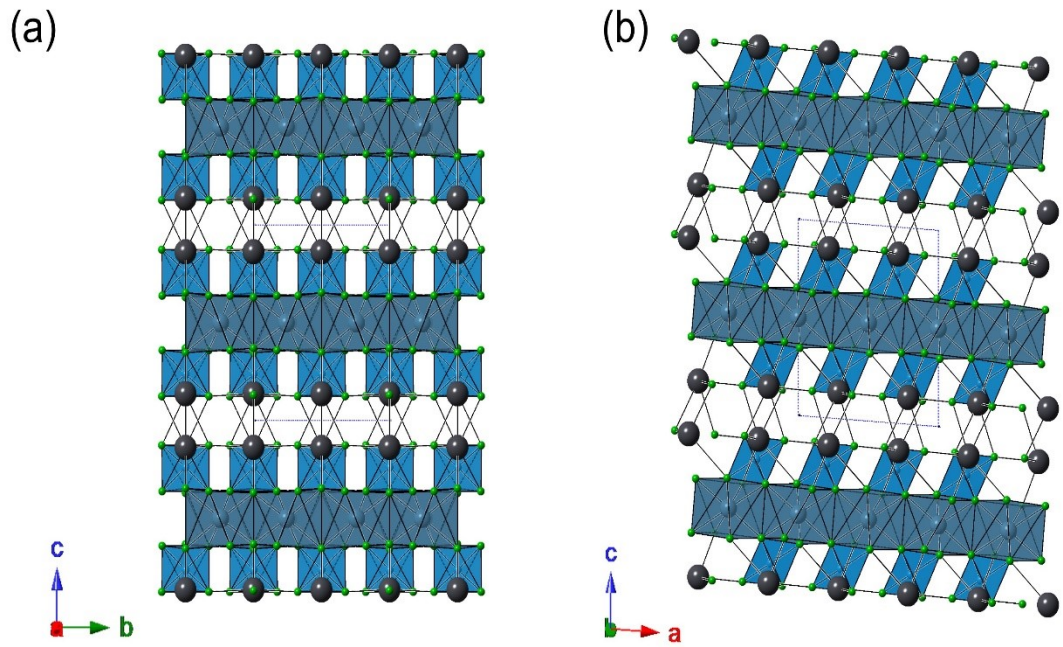

Figure 4. Crystal structure of manuelarossiite as seen down **a** and **b** (in Fig. 4a and b, respectively). Lead and F atoms are shown as dark grey and green circles, respectively, whereas Ca- and Al-centered polyhedra are shown as blue and light blue polyhedra, respectively.

https://doi.org/10.1180/mgm.2024.59 Published online by Cambridge University Press

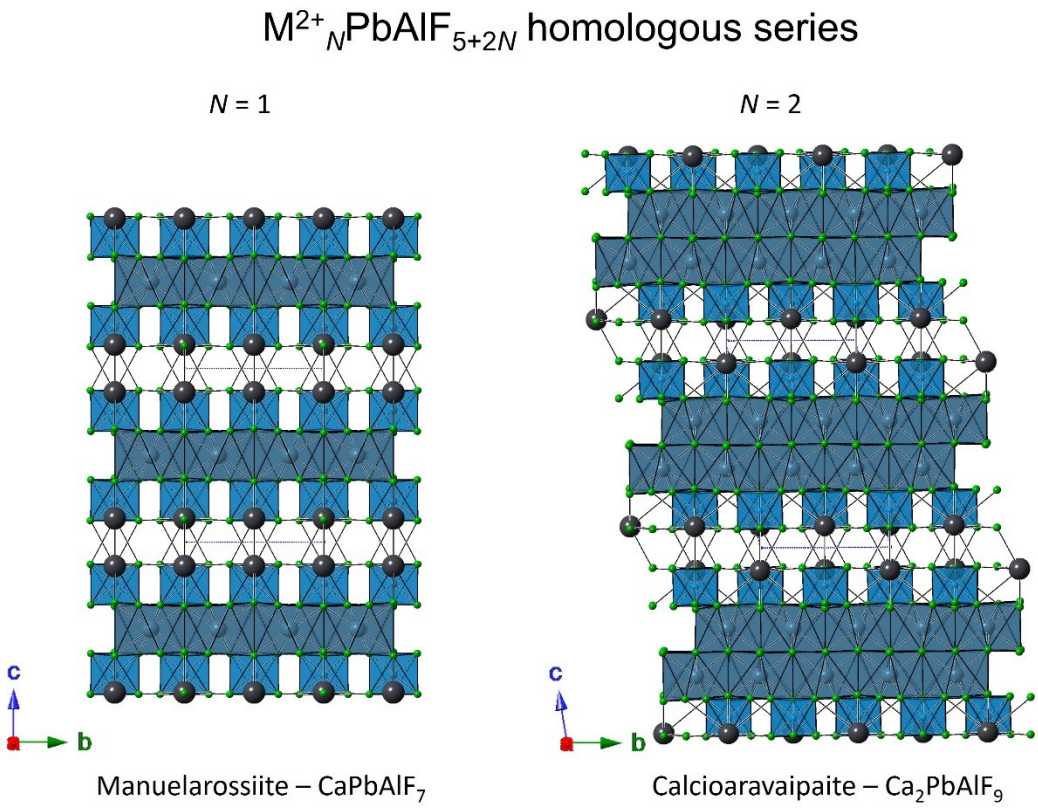

Figure 5. Structural relations between manuelarossiite, aravaipaite and calcioaravaipaite. Same symbols as in Figure 4.

https://doi.org/10.1180/mgm.2024.59 Published online by Cambridge University Press

Table 1. Chemical composition of manuelarossiite.

Constituent	**Wt.%**	**Range**	**Stand. Dev.**	**Reference material**
CaO	13.98	13.95–14.04	0.04	fluorapatite
PbO	55.46	54.80–56.84	0.77	alamosite
Al_2O_3	12.59	12.30–12.72	0.16	almandine
F	29.45	29.39–29.48	0.03	topaz
H_2O*	1.68			
–O = F	–12.40			
Total	**100.76**			
* calculated by stoichiometry				

https://doi.org/10.1180/mgm.2024.59 Published online by Cambridge University Press

Table 2. Powder X-ray diffraction data (*d* in Å) of manuelarossiite compared to the calculated pattern from single-crystal data.

d_{obs}	I_{obs}	d_{calc}*	I_{calc}*	*h k l*
9.257	**57**	9.265	78	0 0 1
5.341	10	5.338	7	1 1 0
4.724	30	4.724	35	1 1 −1
4.537	**72**	4.532	79	1 1 1
3.832	42	3.829	49	2 0 0
3.725	**98**	3.722	74	0 2 0
3.630	**57**	3.627	100	2 0 −1
3.588	**65**	3.584	81	1 1 −2
3.460	**100**	3.454	83	0 2 1
3.422	**63**	3.419	96	1 1 2
3.091	55	3.088	43	0 0 3
2.905	20	2 902	23	0 2 2
2.859	25	2.857	30	2 0 2
2.733	30	2.730	36	1 1 −3
2.673	**65**	2.669	55	2 2 0
2.623	35	2.620	8	1 1 3
2.600	28	2.598	34	2 2 −1
2.420	33	2.414	14	3 1 0
2.380	18	2.377	14	0 2 3
2.319	22	2.316	31	0 0 4
2.302	15	2.300	20	3 1 1
2.280	37	2.276	50	1 3 1
2.201	32	2.200	42	3 1 −2
2.122	5	2.121	16	1 3 −2
		2.089	7	1 1 4
2.088	43	2.086	33	3 1 2
2.070	20	2.069	36	2 2 −3
2.047	12	2.045	16	2 0 −4
1.971	37	1.973	35	2 2 3
1.966	13	1.967	27	0 2 4
		1.965	13	3 1 −3
1.921	7	1.924	8	2 0 4
		1.914	7	4 0 0
1.897	12	1.895	26	1 3 −3
1.864	22	1.861	21	0 4 0
1.816	5	1.814	7	4 0 −2
1.780	12	1.779	7	3 3 0
		1.777	11	1 1 −5
1.732	20	1.732	11	3 3 1
1.694	25	1.693	28	4 2 −1
1.658	13	1.656	19	2 4 −1

*The calculated pattern was obtained using the crystal structure data in Table 4 and the software Vesta (Momma and Izumi, 2011). Only reflections with intensities > 5 and up to 1.656 Å are reported.

https://doi.org/10.1180/mgm.2024.59 Published online by Cambridge University Press

Table 3. Summary of crystal data and parameters describing data collection and refinement for manuelarossiite.

Crystal data	
Crystal size (mm)	0.044 × 0.028 × 0.005
Cell setting, space group	Monoclinic, *C*2/*m*
a (Å)	7.6754(3)
b (Å)	7.4443(4)
c (Å)	9.2870(5)
β (°)	93.928(5)
V (Å^3)	529.39(5)
Z	4
Data collection and refinement	
Radiation, wavelength (Å)	Mo *K*α, λ = 0.71073
Temperature (K)	293(2)
$2\theta_{max}$ (°)	63.14
Measured reflections	7019
Unique reflections	911
Reflections with $F_o > 4\sigma(F_o)$	431
R_{int}	0.0673
$R\sigma$	0.0332
Range of *h*, *k*, *l*	$-11 \le h \le 11$, $-10 \le k \le 10$, $-13 \le l \le 13$
R [$F_o > 4\sigma(F_o)$]	0.0561
R (all data)	0.0611
wR (on F_o^2)*	0.1572
Goof	1.192
Number of least-squares parameters	58
Maximum and minimum residual peak (e Å^{-3})	7.63 [at 1.11 Å from F(2)] −3.59 [at 1.40 Å from F(4)]

*$w = 1/[\sigma^2(F_o^2)+0.0455P^2+103.7547P]$, where $P = (F_o^2+2F_c^2)/3$

https://doi.org/10.1180/mgm.2024.59 Published online by Cambridge University Press

Table 4. Sites, Wyckoff positions, site occupancy factors (s.o.f.), fractional atomic coordinates and equivalent isotropic displacement parameters (Å^2) for manuelarossiite.

Site	*Wyckoff position*	*s.o.f.*	*x/a*	*y/b*	*z/c*	U_{eq}
Pb(1a)	4*i*	$Pb_{0.963(3)}$	0.21596(12)	½	0.86324(10)	0.0200(3)
Pb(1b)	4*i*	$Pb_{0.037(3)}$	0.366(3)	½	0.860(3)	0.0200(3)
Ca	4*h*	$Ca_{1.00}$	0	0.2578(5)	½	0.0122(7)
Al	4*i*	$Al_{1.00}$	0.3014(8)	½	0.2374(7)	0.0142(12)
F(1)	4*i*	$F_{1.00}$	0.0988(18)	½	0.6299(14)	0.018(3)
F(2)	4*i*	$F_{1.00}$	0.0997(16)	½	0.1311(14)	0.019(3)
F(3)	4*i*	$F_{1.00}$	0.5108(19)	½	0.3464(14)	0.020(3)
F(4)	8*j*	$F_{1.00}$	0.2352(11)	0.3284(13)	0.3606(10)	0.0185(18)
F(5)	8*j*	$F_{1.00}$	0.3839(14)	0.3263(15)	0.1254(11)	0.027(2)

https://doi.org/10.1180/mgm.2024.59 Published online by Cambridge University Press

Table 5. Selected bond distances (Å) for manuelarossiite.

Pb(1a)	–F(1)	2.288(13)	Pb(1b)	–F(3)	2.20(3)
	–F(2)	2.427(13)		–F(5)	2.31(2) ×2
	–F(5)	2.551(12) ×2		–F(5)	2.77(2) ×2
	–F(2)	2.700(13)		–F(1)	2.86(3)
	–F(3)	2.958(14)		–F(5)	3.103(18) ×2
	–F(5)	2.972(11) ×2		–F(4)	3.252(18) ×2
	–F(4)	3.248(10) ×2		–F(2)	3.35(3)
	–F(5)	3.327(11) ×2			
Pb(1a)	–Pb(1b)	1.15(2)			
Ca	–F(1)	2.271(9) ×2	Al	–F(2)	1.778(14)
	–F(4)	2.352(9) ×2		–F(5)	1.802(11) ×2
	–F(3)	2.396(9) ×2		–F(4)	1.811(10) ×2
	–F(4)	2.420(9) ×2		–F(3)	1.840(16)

Table 6. Weighted bond-valence sums (in valence unit) for manuelarossiite.

Site	**F(1)**	**F(2)**	**F(3)**	**F(4)**	**F(5)**	**Σcations**	**Theor.**
Pb(1a)	0.48	0.33 0.16	0.08	$0.04^{\times 2\rightarrow}$	$0.24^{\times 2\rightarrow}$ $0.08^{\times 2\rightarrow}$ $0.03^{\times 2\rightarrow}$	1.83	1.93
Pb(1b)			0.02		$0.02^{\times 2\rightarrow}$	0.06	0.07
Ca	$^{\times 2\downarrow}0.31^{\times 2\rightarrow}$		$^{\times 2\downarrow}0.22^{\times 2\rightarrow}$	$0.25^{\times 2\rightarrow}$ $0.21^{\times 2\rightarrow}$		1.98	2.00
Al		0.54	0.45	$0.49^{\times 2\rightarrow}$	$0.50^{\times 2\rightarrow}$	2.97	3.00
Σanions	1.10	1.03	0.99	0.99	0.87		
Theor.	1.00	1.00	1.00	1.00	1.00		

https://doi.org/10.1180/mgm.2024.59 Published online by Cambridge University Press

Table 7. Comparison between currently known Pb-Al fluorides.

Mineral	Manuelarossiite	Aravaipaite		Calcioaravaipaite		Artroeite
Chemical formula	$[CaF_2]PbAlF_5$	$2[PbF_2]PbAlF_5(H_2O)$		$2[CaF_2]PbAlF_5$		$PbAlF_3(OH)_2$
Space group	*C*2/*m*	$P2_1/n$	*P*−1	*C*−1	*P*−1	*P*−1
a (Å)	7.68	25.05	5.66	7.72	5.38	6.27
b (Å)	7.44	5.85	5.86	7.52	5.38	6.82
c (Å)	9.29	5.68	12.70	12.21	12.20	5.06
α (°)	90	90	98.7	98.9	91.4	90.7
β (°)	93.9	94.0	94.0	96.9	101.1	107.7
γ (°)	90	90	90.7	90.0	91.5	104.5
V (Å^3)	529.4	829.7	416.0	694.8	346.7	198.6
Z	4	4	2	4	2	2
Ref.	[1]	[2]	[3]	[4]	[3]	[5]

[1] this work; [2] Kampf (2001); [3] Kampf *et al.* (2011); [4] Kampf *et al.* (2003); [5] Kampf and Foord (1995

https://doi.org/10.1180/mgm.2024.59 Published online by Cambridge University Press